Dyes and Pigments 207 (2022) 110700

Contents lists available at ScienceDirect

Dyes and Pigments

journal homepage: www.elsevier.com/locate/dyepig

Effect of seven different terthiophene π-spacers on dye performance in dye-sensitized solar cells

David Moe Almenningen [a], Henrik Erring Hansen [b], Audun Formo Buene [c], Bård Helge Hoff [a], Odd Reidar Gautun [a,*]

[a] Department of Chemistry, Norwegian University of Science and Technology, Høgskoleringen 5, 7491, Trondheim, Norway
[b] Department of Materials Science and Engineering, Norwegian University of Science and Technology, Sem Sælands vei 12, 7491, Trondheim, Norway
[c] Department of Civil and Environmental Engineering, Norwegian University of Science and Technology, Høgskoleringen 7a, 7034, Trondheim, Norway

ARTICLE INFO

Keywords:
Oligothiophene
Triarylamine dye
Dye-sensitized solar cells
Terthiophene
Cu redox shuttle

ABSTRACT

To ensure high photocurrents from dye-sensitized solar cells (DSSC), it is important that the dye absorbs as much of the energy from the sunlight as possible. To achieve a wide absorption and cover larger parts of the solar spectrum, dyes are frequently fitted with oligothiophene π-spacers. We wish to examine the terthiophene motif as π-spacers in triarylamine dyes and evaluate the suitability of using these in modern copper based DSSC devices. The foundation for this analysis will be the series of seven novel dyes (**DMA-6** – **DMA-12**) which all are fitted with the same donor and acceptor, but linked with seven different terthiophene motifs. The photovoltaic performance of the dyes show that the smallest π-spacer in the series, dithieno[3,2-b:2′,3′-d]thiophene, was the most efficient. The DSSC device sensitized by this dye achieved a power conversion efficiency of 4.4% (J_{sc} = 7.0 mA cm^{-2}, V_{oc} = 0.95 V, FF = 0.66). The photovoltaic performance of the dyes was tested in devices with two different TiO_2 thicknesses, and we established that the thinner TiO_2 yielded the best DSSC performance for all the dyes. Electrochemical impedance spectroscopy revealed that the thicker semiconductor layer resulted in a reduction of the effective electron diffusion length.

1. Introduction

The dye-sensitized solar cell (DSSC), first reported by O'Regan and Grätzel back in 1991 [1], is a photovoltaic technology with an impressive ability to tune properties such as color, transparency, and flexibility. The ability to tune color and transparency have made the DSSC a desirable technology for use in building-integrated photovoltaics [2,3]. While the tunable flexibility has been successfully utilized for integrating the DSSC in wearable devices [4]. More than 30 years of research and development on the DSSC technology have led to devices that vary greatly in materials and methods used in the fabrication of DSSC devices. It is however still possible to identify three key components present in a typical DSSC device, i) the semiconducting mesoporous metal oxide, commonly TiO_2 ii) the sensitizer coating the metal oxide responsible with light harvesting and electron injection into the TiO_2 iii) the redox shuttle responsible with regenerating the oxidized sensitizer [5]. Recent advances have been made on developing copper-based redox shuttles [6]. These severely reduced overpotential losses that previously plagued the DSSC devices operating with iodine redox shuttles. DSSCs utilizing the novel copper complexes have recently become the most efficient technology for ambient light photovoltaics [7,8], making it a very promising energy source for electronics requiring low power.

To successfully take advantage of the novel copper electrolyte, there are certain requirements needed in the design of sensitizers. The redox potentials of the most common copper complexes are found in the range 0.87–0.97 V *vs.* standard hydrogen electrode (SHE) [6], significantly higher than that of the I^-/I_3^- redox shuttle at around 0.40 V *vs.* SHE [9]. This requires the design of dyes with oxidation potentials that are high enough to be regenerated by the copper complexes, and it has been shown that a 10 mV driving force for regeneration is sufficient [6]. Replacing the two-electron redox shuttle I^-/I_3^- with one-electron metal complexes led to a facilitation of the recombination of electrons in the TiO_2 with oxidants in the redox shuttle [10,11]. This required dyes to be designed with alkyl chains that provide an insulating effect and prevents the redox complexes from approaching the TiO_2 surface. The tetra-alkoxy substituted triarylamine donor, referred to as the Hagfeldt

* Corresponding author.
E-mail address: odd.r.gautun@ntnu.no (O.R. Gautun).

https://doi.org/10.1016/j.dyepig.2022.110700
Received 29 June 2022; Received in revised form 26 August 2022; Accepted 27 August 2022
Available online 3 September 2022

donor, is a molecular motif that meets these two requirements expertly [12]. This donor provides excellent shielding of the TiO_2 surface and the reduction in electron recombination has allowed for devices with excellent photovoltages [8]. The downside of the triarylamine dyes is the limited light harvesting ability compared to other donors such as ullazine [13]. To improve the absorption properties of triarylamine dyes, they are frequently fitted with large π-spacers to improve the photocurrent [11,14,15].

In our previous study on π-spacers we found that the terthiophene π-spacer produced the highest photocurrent in dyes employing a phenothiazine donor [16]. Terthiophene is a simple oligothiophene unit comprised of three thiophenes, and over the years numerous variations of terthiophene motifs have been incorporated in dyes for DSSC [17–24]. To exploit the terthiophene light harvesting ability in a copper based DSSC device, we prepared a novel series of dyes with the Hagfeldt donor. Identifying important dye structure-performance relationships in the field of DSSC is difficult, since most studies focus on only a few dyes, and there is significant variation in data for the same dye [25]. We have previously demonstrated the merit of synthesizing dye libraries to investigate various aspects of dye design such as π-spacers [26–29], auxiliary donors [30–32], or dye geometries [33,34]. Therefore, we designed and synthesized seven novel dyes with different terthiophene motifs, and the structures of the dyes are shown in Fig. 1. With dyes **DMA-6** – **DMA-12** we aimed to investigate the effect of the terthiophene structure on the optoelectronic properties of the sensitizers. We further wanted to identify traits of successful terthiophene π-spacers based on the photovoltaic performance of the dyes.

2. Results and discussion

2.1. Dye synthesis

The dyes reported herein was prepared following the two-step synthesis route shown in Scheme 1. The synthesis is based on the successful convergent/divergent synthesis approach reported by Gabrielsson et al. [11]. A full synthetic account is given in the ESI. The advanced triarylamine donor fragment **1** was prepared as described in our previous report [35]. Compound **1** was coupled to the different π-spacer fragments, **2a-2g**, in a Suzuki-Miyaura cross-coupling. Excluding **2d**, all the π-spacer fragments underwent satisfactory reactions using $Pd(OAc)_2$/-SPhos, and gave the corresponding dye precursors in yields of 22–55%. The brominated ethylenedioxythiophene **2d** decomposed under the initial reaction conditions, which led us to change the catalyst to $PdCl_2$(dppf) and we were able to produce and isolate enough of **3d** to prepare sufficient amounts of the resulting sensitizer **DMA-9**. Following the Knoevenagel condensation procedure reported by Iqbal et al. [36], the finished sensitizers, **DMA-6** – **DMA-12**, were prepared and isolated in yields of 63–99%.

2.2. Photophysical properties

Altering the aromatic system of the π-spacer in D-π-A dyes is known to affect the optical properties of the resulting chromophores [37]. To measure the effect of the various π-spacers on the optical properties of the dyes, we performed UV/Vis spectroscopy on the dyes in a dichloromethane solution (2×10^{-5} M) and on dye-stained TiO_2 electrodes (2.5 μm, 18NR-T, Greatcell Solar). The results from these measurements are shown in Fig. 2, and an overview of the obtained data is given in Table 1. In solution, the standard terthiophene-linked dye, **DMA-6**, display an absorption maximum of 481 nm. Remarkably, the absorption maxima of four of the other dyes (**DMA-7**, **DMA-8**, **DMA-11**, **DMA-12**) are found within 4 nm of the standard dye, **DMA-6**. This is surprising considering that the aromatic system of **DMA-7** and **DMA-8** contains two fewer p-electrons and for **DMA-12** it contains four fewer p-electrons. The resulting aromatic system is more planar however, and this is likely the reason why the absorption is not blueshifted by the

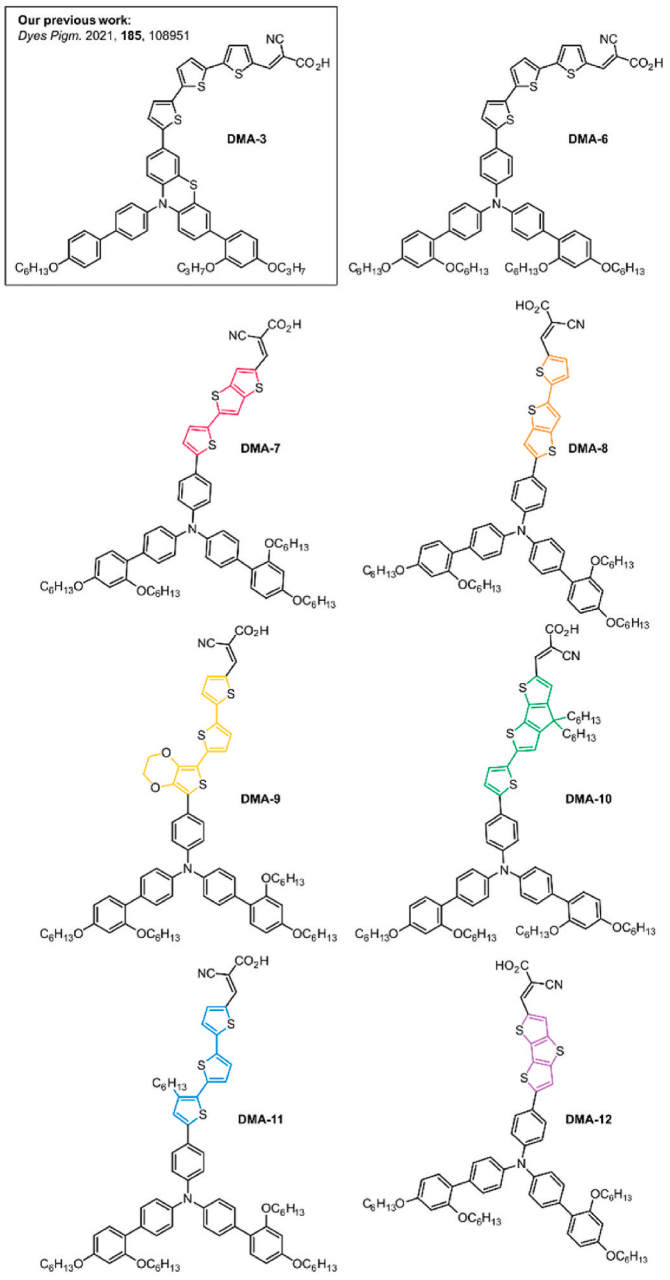

Fig. 1. The structure of the seven novel dyes **DMA-6** – **DMA-12**, and the previously investigated dye, **DMA-3**.

smaller π-spacers. Another striking effect of planarizing the aromatic system is seen for the dye **DMA-10**, where the absorption maxima of this dye is redshifted 61 nm compared to the standard terthiophene dye (**DMA-6**). The molar extinction coefficient of this dye (55,900 M^{-1} cm^{-1}) is also significantly higher than the other dyes in this series, and comparable to that of the benchmark dye **Y123** (57,300 M^{-1} cm^{-1}). We also see that substituting one thiophene for ethylenedioxythiophene is a successful strategy for redshifting absorption, as the absorption maxima of **DMA-9** is 22 nm redshifted compared to **DMA-6**. The redshift can be explained by the increased electron donating ability of the ethylenedioxythiophene compared to thiophene. It is also likely that there are non-covalent S–O interactions occurring between ethylenedioxythiophene and the neighboring thiophene. Such interactions have previously been shown to provide conformational locks and increase the planarity of the aromatic system [38,39].

The absorption maxima were blueshifted for all the dyes when

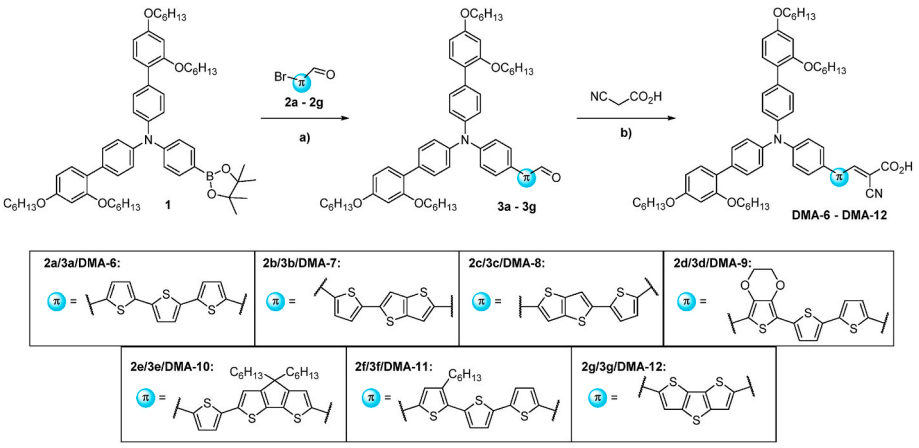

Scheme 1. Our two-step synthesis route for the preparation of dyes **DMA-6** – **DMA-12**. a) Suzuki Miyaura cross-coupling catalyzed by either $Pd(OAc)_2$/SPhos or $PdCl_2$(dppf) (17–55%). b) Knoevenagel condensation mediated by piperidine (63–99%).

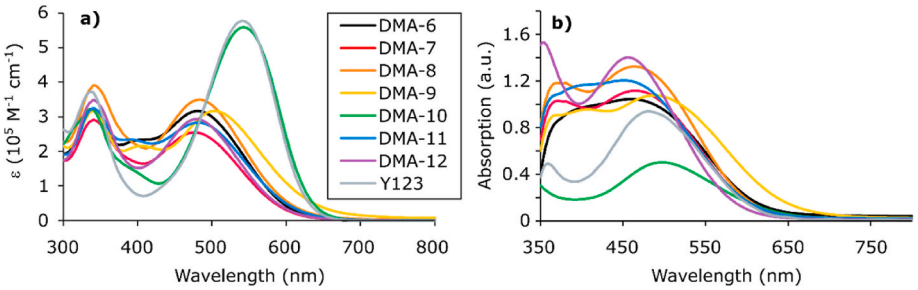

Fig. 2. Absorption spectra of all dyes a) in dichloromethane solution, b) on TiO_2 films (2.5 μm, 18NR-T, Greatcell Solar).

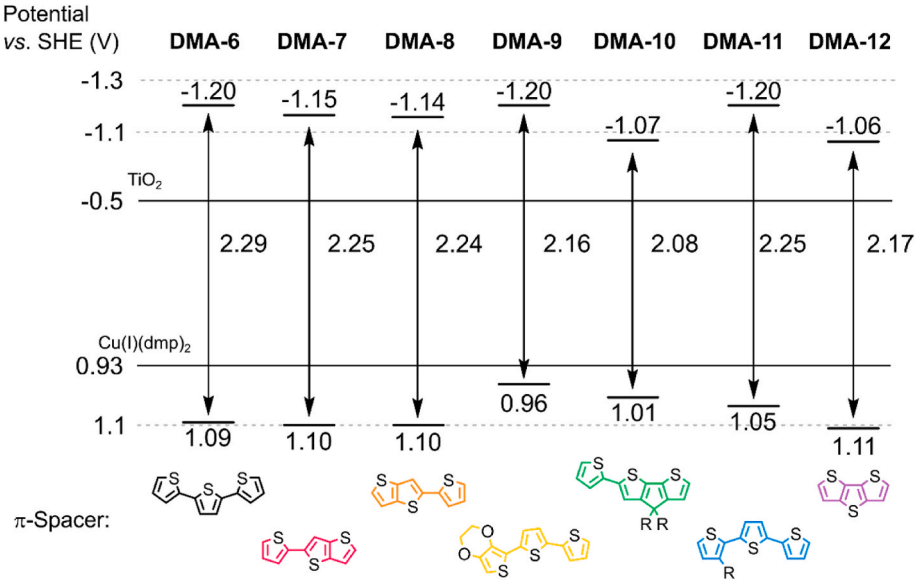

Fig. 3. Energy levels of the frontier orbitals for the sensitizers in this study, R = C_6H_{13}.

comparing the UV/Vis spectra of the stained TiO_2 electrodes to the spectra obtained in dichloromethane solution. Attaching dyes on TiO_2 is frequently associated with blueshifts of absorption, the deprotonation of the anchoring groups and the formation of H-aggregates are the likely causes for this behavior [17,40]. The absorption maximum of the dye **DMA-10** was blueshifted the most upon being absorbed on TiO_2. Despite this, the absorption maximum of 498 nm was the highest of the dyes in this series, in addition it was also redshifted compared to the benchmark dye **Y123** (481 nm). The ethylenedioxythiophene unit is also highly successful in extending the light harvesting region of the dye, as demonstrated by the significantly redshifted absorption onset of **DMA-9** on TiO_2.

To further investigate the effect of the different π-spacers we calculated the optical band gaps, $E_{0\text{-}0}$, from the intersection between the normalized absorption and emission spectra shown in Fig. S1. The unmodified terthiophene dye, **DMA-6**, display a band gap of 2.29 eV which

is consistent with our previously reported terthiophene dye (**DMA-3**) with a band gap of 2.38 eV [16]. We also see that all the other terthiophene motifs reported in this paper produce smaller optical band gaps than the reference dye **DMA-6**. The two structural isomers **DMA-7** and **DMA-8** display similar optical band gaps, showing that the position of the fused bithiophene unit does not affect the band gap of the chromophore. By employing a fully fused terthiophene π-spacer, as seen for **DMA-12**, the band gap is reduced further to 2.17 eV. The most pronounced effect is seen for the cyclopentadithiophene modified dye, **DMA-10**, where the optical band gap is 0.21 eV smaller than the reference dye **DMA-6**.

2.3. Electrochemical properties

Alterations of the aromatic system of D-π-A dyes are likely to affect the electronic properties as well as the optical properties. To quantify this effect, we carried out cyclic voltammetry (CV) experiments on stained TiO_2 electrodes for all the dyes in the series. The obtained voltammograms are shown in Fig. S2, and the energy levels of the frontier orbitals are found in Table 1 and shown in Fig. 3. The oxidation potential of the reference dye, **DMA-6**, was found at 1.09 V *vs*. SHE. This demonstrates the benefit of switching from a phenothiazine donor to a triarylamine donor, as our previously reported terthiophene dye displayed a 13 mV lower oxidation potential [16]. Four other dyes (**DMA-7**, **DMA-8**, **DMA-11**, **DMA-12**) were all found within 4 mV of the reference dye and with sufficient driving force for regeneration with a Cu $(dmp)_2^{1+/2+}$ based redox shuttle (redox potential of 0.93 V *vs*. SHE) [6]. The dye **DMA-10**, with its oxidation potential of 1.01 V *vs*. SHE, is narrowly outside of the 10 mV driving force potential that has been shown previously to be sufficient [6]. While the dye **DMA-9** has an oxidation potential (0.96 V *vs*. SHE) that is expected to be too low to be effectively regenerated by $Cu(dmp)_2^{1+/2+}$. By employing these dyes in DSSCs with a $Cu(dmp)_2^{1+/2+}$ based redox shuttle we will further investigate the driving force requirements for this electrolyte.

2.4. Photovoltaic properties

The photovoltaic performance of the different sensitizers in this study was measured by preparing DSSC devices sensitized by each dye.

Table 1
Photophysical and electrochemical properties of dyes in the series.

Dye	λ_{abs} [a] (nm)	ε ($M^{-1}cm^{-1}$)	Em. [b] (nm)	λ_{abs} [c] on TiO_2 (nm)	$E_{0\text{-}0}$ [d] (eV)	E_{ox} [e] (V *vs*. SHE)	E_{LUMO} [f] (V *vs*. SHE)
DMA-6	481	31,700	600	459	2.29	1.09	−1.20
DMA-7	477	25,500	614	465	2.25	1.10	−1.15
DMA-8	483	35,000	618	464	2.24	1.10	−1.14
DMA-9	503	31,700	632	488	2.16	0.96	−1.20
DMA-10	542	55,900	691	498	2.08	1.01	−1.07
DMA-11	481	28,300	635	451	2.25	1.05	−1.20
DMA-12	479	29,400	705	456	2.17	1.11	−1.06

[a] Maximum of most redshifted peak.
[b] Emission when ICT band is excited, in DCM solution.
[c] Maximum of most redshifted peak on TiO_2 (2.5 μm, GreatcellSolar 18NR-T).
[d] Calculated from the intersection of the absorption and normalized emission spectra.
[e] Measured vs. F_c^+/F_c on stained TiO_2 electrodes in acetonitrile with 0.1 M LiTFSI, converted to V vs. SHE by 0.624 V. Scan rate 10 mV s^{-1}
[f] Calculated from E_{ox}-$E_{0\text{-}0}$.

The results from these measurements are given as averages of three devices in Table 2, and the *J-V* curve of the best performing device for each dye is shown in Fig. 4. We have previously demonstrated the benefit of increasing the thickness of the active TiO_2 layers in DSSCs employing copper redox shuttles [35]. Based on this, we set out to prepare devices with varying film thickness of the active 30NR-D TiO_2 layer (4.5 μm and 9.0 μm) while keeping the thickness of the scattering WER2-O TiO_2 layer fixed (4.5 μm).

Based on the series of dyes **DMA-6** – **DMA-12**, we can identify certain successful traits in the various terthiophene designs. There is a massive benefit in putting the thieno [3,2-b]thiophene unit on the donor side of the π-spacer, as demonstrated by comparing the photovoltaic performance of the structural isomers **DMA-7** and **DMA-8**. When we examine

Table 2
Photovoltaic performance of all dyes under 1 sun AM 1.5G illumination, given as averages of three separate DSSC devices. Along with the integrated current density from IPCE measurements. Results from dye loading experiments is also included.

Dye	TiO_2 (μm) [a]	IPCE J_{sc} (mA cm^{-2}) [b]	J_{sc} (mA cm^{-2})	V_{oc} (V)	FF	PCE (%)	Dye loading (10^{-8} mol cm^{-2}) [c]
DMA-6	4.5	7.54	6.1 ± 0.2	0.89 ± 0.01	0.61 ± 0.05	3.3 ± 0.2	8.4 ± 0.4
	9	6.74	5.0 ± 0.3	0.85 ± 0.00	0.66 ± 0.00	2.8 ± 0.2	17.5 ± 0.3
DMA-7	4.5	5.58	5.1 ± 0.2	0.87 ± 0.00	0.63 ± 0.05	2.8 ± 0.3	8.9 ± 0.9
	9	5.82	4.3 ± 0.2	0.84 ± 0.00	0.65 ± 0.05	2.4 ± 0.2	11.5 ± 0.3
DMA-8	4.5	7.25	6.4 ± 0.3	0.91 ± 0.00	0.59 ± 0.02	3.4 ± 0.2	10.5 ± 1.1
	9	7.75	5.7 ± 0.2	0.86 ± 0.01	0.64 ± 0.02	3.1 ± 0.1	13.1 ± 1.7
DMA-9	4.5	4.50	3.1 ± 0.4	0.78 ± 0.01	0.55 ± 0.04	1.3 ± 0.2	7.3 ± 0.4
	9	2.84	2.3 ± 0.0 [d]	0.75 ± 0.01 [d]	0.48 ± 0.01 [d]	0.8 ± 0.0 [d]	22.2 ± 0.5
DMA-10	4.5	6.84	5.9 ± 0.2	0.83 ± 0.00	0.68 ± 0.00	3.3 ± 0.1	12.5 ± 1.6
	9	7.00	5.7 ± 0.1	0.81 ± 0.00	0.65 ± 0.01	3.0 ± 0.0	17.4 ± 0.3
DMA-11	4.5	8.77	7.0 ± 0.0	0.94 ± 0.00	0.62 ± 0.01	4.1 ± 0.1	11.3 ± 0.5
	9	7.12	5.5 ± 0.5	0.86 ± 0.01	0.52 ± 0.01	2.5 ± 0.3	23.2 ± 0.1
DMA-12	4.5	8.32	7.0 ± 0.2	0.95 ± 0.02	0.66 ± 0.01	4.4 ± 0.2	12.2 ± 0.6
	9	6.11	4.1 ± 0.3	0.83 ± 0.01	0.41 ± 0.02	1.4 ± 0.1	14.1 ± 1.2
Y123 [e]	4.5	11.30	9.9	0.95	0.68	6.4	13.8 ± 0.9
	9	11.30	8.8	0.93	0.58	4.7	18.6 ± 0.2

[a] Thickness of active 30 NR-D layer, the scattering WER2-O layer was fixed at 4.5 μm.
[b] Obtained by integration of the IPCE spectrum over the 1 sun AM 1.5 G spectrum.
[c] Values averaged of two desorbed TiO_2-electrodes.
[d] Average values of two cells.
[e] Values from best-performing device.

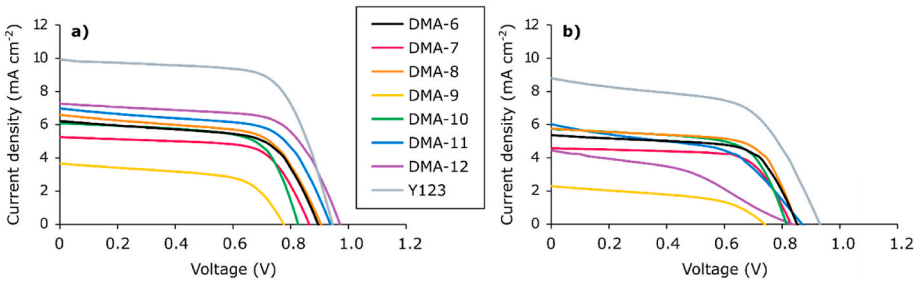

Fig. 4. J-V curves for the best parallel of each dye, obtained under 1 sun AM 1.5G illumination a) 4.5 μm TiO_2 devices b) 9 μm TiO_2 devices.

the incident photon-to-current efficiency (IPCE) spectra, shown in Fig. 5, we see that the dye **DMA-8** outperforms its analog throughout the entire range of wavelengths. This translates to an improvement in J_{sc} from 5.1 to 6.4 mA cm^{-2} (25% improvement) in the thin TiO_2 devices, and an improvement from 4.3 to 5.7 mA cm^{-2} (33% improvement) in the thicker TiO_2. Under the optimal thin TiO_2 conditions, the hexyl substituted terthiophene (**DMA-11**) yielded an 24% increase in PCE compared to the non-modified terthiophene (**DMA-6**). Under the same conditions, the fully fused terthiophene of **DMA-12** improved the PCE by 33% compared to the standard terthiophene of **DMA-6**. The dye **DMA-12** under thin film conditions proved to be the most efficient device in the series, delivering a PCE of 4.4% (J_{sc} = 7.0 mA cm^{-2}, V_{oc} = 0.95 V, FF = 0.66).

Conversely, the PCE data of this series of dyes also highlights terthiophene design concepts to avoid in the future. This is perhaps most striking when we consider that the performance of the dyes in this series was also compared to the known benchmark dye **Y123,** which in molecular structure closely resembles the dye **DMA-10**. The only difference between these two dyes is that **Y123** has one thiophene less in the π-spacer. Although the absorption properties of **DMA-10** are similar to that of **Y123** in solution, and the dye loading of these dyes are similar, this does not translate into improved short-circuit current (J_{sc}) for the larger dye. The larger π-spacer of **DMA-10** leaves it more susceptible to aggregate than the more concise dye **Y123.** This could be part of the reason why the photovoltaic performance drops so severely by the introduction of an additional thiophene in the π-spacer of **DMA-10**. The formation of H-aggregates when dyes are sensitized on TiO_2 is known to blueshift absorption and also promote excited state quenching [41], both of which are deleterious for solar cell performance. The extra thiophene unit also lowered the oxidation potential from 1.07 V *vs.* SHE for **Y123** to 1.01 V vs. SHE for **DMA-10**, which leaves the driving force for regeneration of the latter dye at only 8 mV in the redox shuttle employed in this study. A large number of oxidized dye molecules not being effectively regenerated, is expected to contribute to the low J_{sc} produced by a dye with such a wide range of absorption as **DMA-10**. The effect of low oxidation potentials is even more apparent when we consider the photovoltaic performance of the dye **DMA-9**, which has a mere 3 mV driving force for regeneration. To investigate whether this was the case, we prepared devices based on **DMA-9** and **DMA-10** but this time with an I^-/I_3^- redox shuttle. The results from these measurements are shown in Table S1. For **DMA-9** a doubled short-circuit current was observed, the dye **DMA-10** also produced improved photocurrents under these conditions. The improved photocurrents suggest that the driving force for regeneration was a bottleneck for the copper regenerated DSSCs. Despite possessing improved absorption properties in solution and while sensitized on TiO_2 compared to the other dyes in the series, the dye **DMA-9** produces the lowest J_{sc}-values of all the dyes reported herein. As a result, the photovoltaic performance of the dye **DMA-9** is by far the worst, and highlights the importance of dyes having oxidation potentials that matches the redox shuttle.

In a recent paper by Velore et al. [42] they highlight the potential pitfalls of using thicker TiO_2 layers and copper redox shuttles together, under 1 sun illumination this strategy can lead to devices suffering from mass transport issues. The results obtained herein support this finding, as all the dyes perform better in the thin TiO_2 devices. The two most efficient dyes, **DMA-11** and **DMA-12**, were also the dyes that displayed the most drastic decrease in performance when going from a thinner active TiO_2 layer to a thicker one. This suggest that these two dyes suffer the most from mass transport issues in a 9 μm TiO_2 device, which could indicate that they form the most closely packed dye layers and limit the movement of the redox shuttle the most. A curious observation concerning these two dyes, is the fact that the dye loading of **DMA-11** more than doubled in going from a thin to a thick TiO_2 layer. While only a small increase in dye loading of **DMA-12** was observed from the same modification. This shows that while the dye structure is important for dye loading, the formation of a close-packed dye layer is not so dependent of a high dye loading.

2.5. *Electrochemical impedance spectroscopy*

To evaluate the influence of TiO_2 thickness on the electron transport properties of the dyes we examined the effective electron diffusion length (L_n), and the results are shown in Fig. 6. The effective electron diffusion length is a measure of the competition between charge collection and charge recombination [43], and is given by

$$L_n = L\sqrt{\frac{R_{rec}}{R_{tr}}} \quad (1)$$

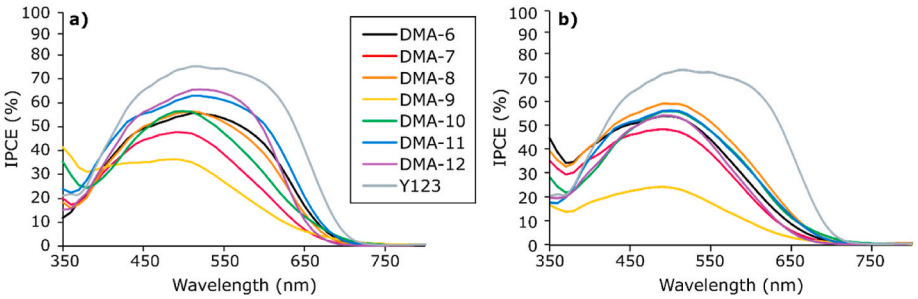

Fig. 5. IPCE spectra of the best performing parallel for each dye a) 4.5 μm TiO_2 devices b) 9 μm TiO_2 devices.

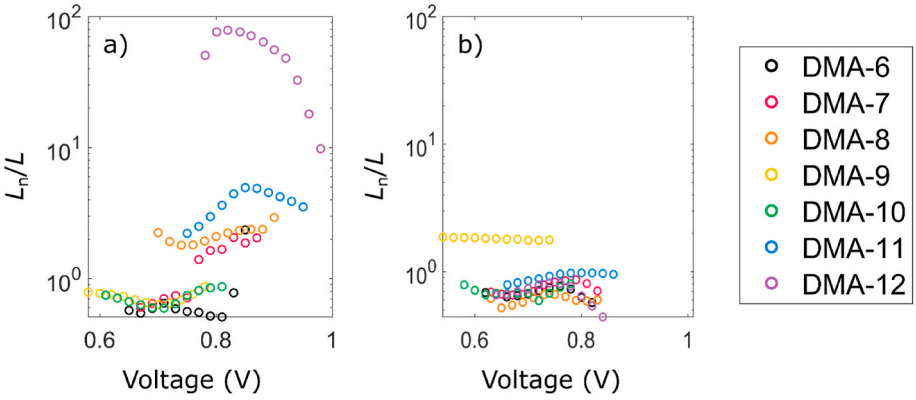

Fig. 6. The ratio of effective electron diffusion length and TiO_2 film thickness a) for 4.5 μm active TiO_2 devices b) for 9 μm active TiO_2 devices.

where L is the film thickness, R_{rec} is the recombination resistance and R_{tr} is the transport resistance. The two resistances were obtained from electrochemical impedance spectroscopy (EIS), and the complex plane plots and resistance data extracted from the EIS measurements are shown in Figs. S3–S6 in the ESI. We see that the dye **DMA-12** in the 4.5 μm TiO_2 devices provide by far the best L_n values of the dyes in this series, which is largely owed to the significantly lower transport resistance in this DSSC device. This could indicate that the smallest π-spacer ensures the highest electron density in the TiO_2, possibly from an increased electron injection efficiency. When considering the effective electron diffusion length of the devices with different TiO_2 film thickness, we see a detrimental effect from the thicker metal oxide layers. Excluding **DMA-9**, all the dyes have reduced L_n values in the thicker TiO_2 devices. The effective electron diffusion lengths displayed in Fig. 6 b) show that these devices are described by Gerischer impedance [44], where the transport resistance is larger than the recombination resistance. This highlights and confirms the need for thinner TiO_2 layers in devices employing copper complex redox shuttles.

3. Conclusion

We have successfully synthesized a series of seven novel dyes with varying terthiophene π-spacer motifs and shown the merit of the convergent/divergent synthesis approach to prepare libraries of dyes. We have demonstrated that reducing the size of the terthiophene aromatic system through fused bithiophenes (**DMA-7** and **DMA-8**) or fused terthiophene (**DMA-12**) does not blueshift the absorption maximum. In addition, all modifications to the terthiophene unit reported herein resulted in a smaller optical band gap compared to the reference sensitizer **DMA-6**. Through photovoltaic characterization, we were able to identify the hexyl-substituted terthiophene (**DMA-11**) and the fully fused terthiophene (**DMA-12**) as the most successful π-spacer motifs. Unfortunately, the dyes displaying the best absorption properties (**DMA-9** and **DMA-10**) had their HOMO energy levels lowered too much to be used effectively in the copper redox shuttle. It is however an exciting prospect to take advantage of the improved absorption of these dyes in devices with redox shuttles that are more compatible such as cobalt complexes. Through EIS experiments we also confirmed the deleterious effect of using thick TiO_2 layers in copper regenerated devices, as all the 9 μm TiO_2 devices showed a Gerischer behavior.

4. Experimental

4.1. Materials and reagents

The donor moiety was prepared following our previously reported procedure [35]. The π-spacers, 5″-bromo[2,2′:5′,2″-terthiophene]-5-carboxaldehyde (**2a**) [16], 5-(5-bromothiophen-2-yl)thieno [3,2-b]thiophene-2-carbaldehyde (**2b**) [45], 5-(5-bromothieno [3,2-b]thiophen-2-yl)thiophene-2-carbaldehyde (**2c**) [46], 5′′-bromo-3′′-hexyl-[2,2′:5′,2′′-terthiophene]-5-carbaldehyde (**2f**) [47], 6-bromodithieno[3,2-b:2′,3′-d]thiophene-2-carboxaldehyde (**2g**) [48], were prepared from literature procedures. The starting material, 6-bromo-4,4-dihexyl-4H-cyclopenta[2,1-b:3,4-b′]dithiophene-2-carbaldehyde, for the synthesis of π-spacer fragment **2e** was prepared according to a literature procedure [49].

The benchmark dye **Y123**, and the copper complexes $Cu^{(I)}(dmp)_2(TFSI)$ and $Cu^{(II)}(dmp)_2(TFSI)_2$ were purchased from Dyenamo AB (Sweden). The remaining chemicals were purchased from Merck (Germany) unless specified otherwise.

4.2. Fabrication of dye-sensitized solar cells

The anodes were prepared from FTO glass (NSG10, Nippon Sheet Glass), which was first cleaned in a Deconex 21-solution (2 g/L) under sonication for 45 min. Next the FTO was treated with UV/O_3 (Novascan PSD PRO-UV T6) for 15 min. Immersion of the glass in aqueous $TiCl_4$-solution (40 mM) at 70 °C for 2 × 45 min followed by rinsing with deionized water and ethanol was carried out to deposit a blocking layer on the FTO-sample. Pastes of TiO_2 were screen printed onto the FTO (mesh count 54, thread diameter 64 mm, area 0.2826 cm^2), for the 4.5 μm devices one active layer (30NR-D, Dyesol) was printed. For the 9 μm devices two active layers were printed with 5 min heating on a hotplate at 125 °C after each layer. A scattering layer (WER2-O, Dyesol) was ultimately printed, and the TiO_2 was sintered in a programmable furnace (Nabertherm LT 9/12) at set temperatures of 125, 250, 325, 450, and 500 °C for 5, 5, 5, 15, and 15 min with a ramping time of 10 min. The thickness of the TiO_2 layers were measured with a Veeco Dektak 150 profilometer. Before staining, the electrodes were annealed at 500 °C for 30 min using a hotplate.

The counter electrodes were prepared from TEC10 FTO glass supplied by Sigma Aldrich. Holes were drilled into the electrodes from the FTO-side using a diamond drill bit, this procedure was carried out under water. The glass plates were then cleaned using Deconex 21 (aq., 2 g/L), deionized water, ethanol, and acetone, in an ultrasonic bath for 15 min for each. A catalytic layer of PEDOT was formed following the electrochemical deposition procedure reported by Ellis et al. [50].

The photoanodes were placed in the dye bath while still holding ~80 °C from the annealing procedure and stored in an oven at 30 °C overnight. The dye baths were prepared using a mixture of *t*-BuOH, MeCN and THF (1:1:1, v/v) to make a solution of dye and co-adsorbent CDCA, at concentrations of 0.1 mM and 1 mM respectively. The staining of the benchmark dye **Y123** was done similarly, but the solvents used was in this case *t*-BuOH and MeCN (1:1, v/v). Following 15 h of staining the electrodes were rinsed in acetonitrile for 2 min, then sealed to the counter electrode using Surlyn (25 μm, Solaronix) in a drybox. A 4 × 20 s

treatment of the cell using a 50 W PTC heat element was sufficient to seal the cells. The electrolyte was vacuum backfilled into the device, the filling-hole was sealed with Surlyn and a glass cover disk, then to complete the devices the electrodes were painted with silver conducting paint (Electrolube, SCP). The electrolyte employed consisted of [Cu(I)(dmp)$_2$]TFSI (0.20 M), [Cu(II)(dmp)$_2$](TFSI)$_2$ (0.10 M), LiTFSI (0.10 M), and *N*-methylbenzimidazole (0.60 M) dissolved in dry acetonitrile.

4.3. Device characterization

J-V curves were obtained under 1 sun illumination AM 1.5G illumination provided by a Sciencetech SP300B solar simulator, calibrated with a Newport Reference Cell (91150V), connected to a Keithley 2450 SourceMeter. A mask with an active area of 0.238 cm^2 was used on all the J-V measurements. IPCE measurements were carried out using a halogen lamp (Ocean Optics HL-2000) and a monochromator (Spectral Products CM110) connected to the Keithley 2450. The devices and the reference photodiode (Thorlabs, FDS100-CAL) were covered with a mask with a size of 0.049 cm^2.

The electrochemical impedance properties were measured in a light-exclusion box containing a Zahner CIMPS QE/IPCE TLS03 tunable light source under constant illumination at wavelength 479 nm with an intensity of 12.6 mW/cm^2. The procedure for these measurements is identical to our previous study [16]. The transmission line model presented by Fagregat-Santiago et al. [51] was used to fit the data obtained from the measurements.

CRediT authorship contribution statement

David Moe Almenningen: Investigation, Methodology, Conceptualization, Writing – original draft, Writing – review & editing, Visualization. **Henrik Erring Hansen:** Investigation, Writing – review & editing, Visualization. **Audun Formo Buene:** Methodology, Writing – review & editing, Visualization. **Bård Helge Hoff:** Supervision, Writing – review & editing. **Odd Reidar Gautun:** Supervision, Conceptualization, Writing – review & editing.

Declaration of competing interest

The authors declare that they have no known competing financial interests or personal relationships that could have appeared to influence the work reported in this paper.

Data availability

No data was used for the research described in the article.

Acknowledgements

The authors acknowledge staff engineer Roger Aarvik and Ph.D. Susana Villa Gonzalez for their technical and mass spectrometry contributions. The support from the Research Council of Norway to the Norwegian NMR Platform (project number 226244/F50) is much appreciated. The Research Council of Norway is acknowledged for the support to the Norwegian Micro- and Nano-Fabrication Facility, NorFab, project number 245963/F50.

Appendix A. Supplementary data

Supplementary data to this article can be found online at https://doi.org/10.1016/j.dyepig.2022.110700.

References

[1] O'Regan B, Grätzel M. A low-cost, high-efficiency solar cell based on dye-sensitized colloidal TiO2 films. Nature 1991;353(6346):737–40.
[2] Yoon S, Tak S, Kim J, Jun Y, Kang K, Park J. Application of transparent dye-sensitized solar cells to building integrated photovoltaic systems. Build Environ 2011;46(10):1899–904.
[3] Grifoni F, Bonomo M, Naim W, Barbero N, Alnasser T, Dzeba I, et al. Toward sustainable, colorless, and transparent photovoltaics: state of the art and perspectives for the development of selective near-infrared dye-sensitized solar cells. Adv Energy Mater 2021;11(43):2101598.
[4] Yun MJ, Cha SI, Seo SH, Lee DY. Highly flexible dye-sensitized solar cells produced by sewing textile electrodes on cloth. Sci Rep 2014;4:5322.
[5] Hagfeldt A, Boschloo G, Sun L, Kloo L, Pettersson H. Dye-sensitized solar cells. Chem Rev 2010;110(11):6595–663.
[6] Saygili Y, Söderberg M, Pellet N, Giordano F, Cao Y, Muñoz-García AB, et al. Copper bipyridyl redox mediators for dye-sensitized solar cells with high photovoltage. J Am Chem Soc 2016;138(45):15087–96.
[7] Cao Y, Liu Y, Zakeeruddin SM, Hagfeldt A, Grätzel M. Direct contact of selective charge extraction layers enables high-efficiency molecular photovoltaics. Joule 2018;2(6):1108–17.
[8] Zhang D, Stojanovic M, Ren Y, Cao Y, Eickemeyer FT, Socie E, et al. A molecular photosensitizer achieves a Voc of 1.24 V enabling highly efficient and stable dye-sensitized solar cells with copper(II/I)-based electrolyte. Nat Commun 2021;12(1):1777.
[9] Kay A, Humphry-Baker R, Graetzel M. Artificial photosynthesis. 2. Investigations on the mechanism of photosensitization of nanocrystalline TiO2 solar cells by chlorophyll derivatives. J Phys Chem 1994;98(3):952–9.
[10] Feldt SM, Gibson EA, Gabrielsson E, Sun L, Boschloo G, Hagfeldt A. Design of organic dyes and cobalt polypyridine redox mediators for high-efficiency dye-sensitized solar cells. J Am Chem Soc 2010;132(46):16714–24.
[11] Gabrielsson E, Ellis H, Feldt S, Tian H, Boschloo G, Hagfeldt A, et al. Convergent/divergent synthesis of a linker-varied series of dyes for dye-sensitized solar cells based on the D35 donor. Adv Energy Mater 2013;3(12):1647–56.
[12] Baumann A, Curiac C, Delcamp JH. The Hagfeldt donor and use of next-generation bulky donor designs in dye-sensitized solar cells. ChemSusChem 2020;13(10):2503–12.
[13] Delcamp JH, Yella A, Holcombe TW, Nazeeruddin MK, Grätzel M. The molecular engineering of organic sensitizers for solar-cell applications. Angew Chem Int Ed 2013;52(1):376–80.
[14] Zhang X, Xu Y, Giordano F, Schreier M, Pellet N, Hu Y, et al. Molecular engineering of potent sensitizers for very efficient light harvesting in thin-film solid-state dye-sensitized solar cells. J Am Chem Soc 2016;138(34):10742–5.
[15] Eom YK, Kang SH, Choi IT, Yoo Y, Kim J, Kim HK. Significant light absorption enhancement by a single heterocyclic unit change in the π-bridge moiety from thieno[3,2-b]benzothiophene to thieno[3,2-b]indole for high performance dye-sensitized and tandem solar cells. J Mater Chem 2017;5(5):2297–308.
[16] Almenningen DM, Hansen HE, Vold MF, Buene AF, Venkatraman V, Sunde S, et al. Effect of thiophene-based π-spacers on N-arylphenothiazine dyes for dye-sensitized solar cells. Dyes Pigments 2021;185:108951.
[17] Tian H, Yang X, Chen R, Zhang R, Hagfeldt A, Sun L. Effect of different dye baths and dye-structures on the performance of dye-sensitized solar cells based on triphenylamine dyes. J Phys Chem C 2008;112(29):11023–33.
[18] Fischer MKR, Wenger S, Wang M, Mishra A, Zakeeruddin SM, Grätzel M, et al. D-π-A sensitizers for dye-sensitized solar cells: linear vs branched oligothiophenes. Chem Mater 2010;22(5):1836–45.
[19] Won YS, Yang YS, Kim JH, Ryu J-H, Kim KK, Park SS. Organic photosensitizers based on terthiophene with alkyl chain and double acceptors for application in dye-sensitized solar cells. Energy Fuels 2010;24(6):3676–81.
[20] Feng Q, Zhang Q, Lu X, Wang H, Zhou G, Wang Z-S. Facile and selective synthesis of oligothiophene-based sensitizer isomers: an approach toward efficient dye-sensitized solar cells. ACS Appl Mater Interfaces 2013;5(18):8982–90.
[21] Feng Q, Zhou G, Wang Z-S. Varied alkyl chain functionalized organic dyes for efficient dye-sensitized solar cells: influence of alkyl substituent type on photovoltaic properties. J Power Sources 2013;239:16–23.
[22] Elmorsy MR, Su R, Fadda AA, Etman HA, Tawfik EH, El-Shafei A. Effect of terthiophene spacer position in Ru(II) bipyridyl complexes on the photocurrent and photovoltage for high efficiency dye-sensitized solar cells. Dyes Pigments 2018;156:348–56.
[23] Elmorsy MR, Su R, Fadda AA, Etman HA, Tawfik EH, El-Shafei A. Co-sensitization of Ru(ii) complex with terthiophene-based D–π–π–A metal-free organic dyes for highly efficient dye-sensitized solar cells: influence of anchoring group on molecular geometry and photovoltaic performance. New J Chem 2018;42(14):11430–7.
[24] Wu Z-S, Song X-C, Liu Y-D, Zhang J, Wang H-S, Chen Z-J, et al. New organic dyes with varied arylamine donors as effective co-sensitizers for ruthenium complex N719 in dye sensitized solar cells. J Power Sources 2020;451:227776.
[25] Buene AF, Almenningen DM. Phenothiazine and phenoxazine sensitizers for dye-sensitized solar cells – an investigative review of two complete dye classes. J Mater Chem C 2021;9(36):11974–94.
[26] Buene AF, Boholm N, Hagfeldt A, Hoff B. Effect of furan π-spacer and triethylene oxide methyl ether substituents on performance of phenothiazine sensitizers in dye-sensitized solar cells. New J Chem 2019;43:9403–10.
[27] Buene AF, Uggerud N, Economopoulos SP, Gautun OR, Hoff BH. Effect of π-linkers on phenothiazine sensitizers for dye-sensitized solar cells. Dyes Pigments 2018;151:263–71.
[28] Gudim NS, Mikhailov MS, Knyazeva EA, Almenningen DM, Mikhalchenko LV, Economopoulos SP, et al. Monitoring the dependence of the photovoltaic properties of dye-sensitized solar cells from the structure of D–A–π–A-type

sensitizers with a 9-(p-tolyl)-2,3,4,4a,9,9a-hexahydro-1H-1,4-methanocarbazole donor building block. Mol Syst Des Eng 2022;7:755–66.
[29] Yemene AE, Venkatraman V, Moe Almenningen D, Hoff BH, Gautun OR. Synthesis of novel 3,6-dithienyl diketopyrrolopyrrole dyes by direct C-H arylation. Molecules 2020;25(10):2349.
[30] Buene AF, Christensen M, Hoff BH. Effect of auxiliary donors on 3,8-phenothiazine dyes for dye-sensitized solar cells. Molecules 2019;24(24):4485.
[31] Buene AF, Ose EE, Zakariassen A, Hagfeldt A, Hoff B. Auxiliary donors for phenothiazine sensitizers for dye-sensitized solar cells – how important are they really? J Mater Chem A 2019;7:7581–90.
[32] Almenningen DM, Haga BS, Hansen HE, Buene AF, Hoff BH, Gautun OR. Adamantyl side-chains as anti-aggregating moieties in dyes for dye-sensitized solar cells. Chem Eur J 2022:e202201726 [Accepted Article].
[33] Buene AF, Hagfeldt A, Hoff BH. A comprehensive experimental study of five fundamental phenothiazine geometries increasing the diversity of the phenothiazine dye class for dye-sensitized solar cells. Dyes Pigments 2019;169:66–72.
[34] Almenningen DM, Engh VM, Strømsodd EA, Hansen HE, Buene AF, Hoff BH, et al. Synthetic efforts to investigate the effect of planarizing the triarylamine geometry in dyes for dye-sensitized solar cells. ACS Omega 2022;7(25):22046–57.
[35] Buene AF, Almenningen DM, Hagfeldt A, Gautun OR, Hoff BH. First report of chenodeoxycholic acid–substituted dyes improving the dye monolayer quality in dye-sensitized solar cells. Sol RRL 2020;4(4):1900569.
[36] Iqbal Z, Wu W-Q, Huang Z-S, Wang L, Kuang D-B, Meier H, et al. Trilateral π-conjugation extensions of phenothiazine-based dyes enhance the photovoltaic performance of the dye-sensitized solar cells. Dyes Pigments 2016;124:63–71.
[37] Bureš F. Fundamental aspects of property tuning in push–pull molecules. RSC Adv 2014;4(102):58826–51.
[38] Lang Y, Chen H, Lai H, Lu Y, Zhu Y, Yu P, et al. Isomeric nonfullerene acceptors: planar conformation leading to a higher efficiency. ACS Appl Energy Mater 2022;5:4556–63.
[39] Zhong J, Cui Y, Zhu P, Zhang M, Xie W, Liu H, et al. Nonfused ring electron acceptors for efficient organic solar cells enabled by multiple intramolecular conformational locks. ACS Appl Energy Mater 2022;5:5136–45.
[40] Dentani T, Kubota Y, Funabiki K, Jin J, Yoshida T, Minoura H, et al. Novel thiophene-conjugated indoline dyes for zinc oxide solar cells. New J Chem 2009;33(1):93–101.
[41] Zhang L, Cole JM. Dye aggregation in dye-sensitized solar cells. J Mater Chem 2017;5(37):19541–59.
[42] Velore J, Chandra Pradhan S, Hamann TW, Hagfeldt A, Unni KNN, Soman S. Understanding mass transport in copper electrolyte-based dye-sensitized solar cells. ACS Appl Energy Mater 2022;5(3):2647–54.
[43] Wang Q, Ito S, Grätzel M, Fabregat-Santiago F, Mora-Seró I, Bisquert J, et al. Characteristics of high efficiency dye-sensitized solar cells. J Phys Chem B 2006;110(50):25210–21.
[44] Wang Q, Moser J-E, Grätzel M. Electrochemical impedance spectroscopic analysis of dye-sensitized solar cells. J Phys Chem B 2005;109(31):14945–53.
[45] Cai S, Tian G, Li X, Su J, Tian H. Efficient and stable DSSC sensitizers based on substituted dihydroindolo[2,3-b]carbazole donors with high molar extinction coefficients. J Mater Chem 2013;1(37):11295–305.
[46] Zhu S, An Z, Chen X, Chen P, Liu Q. Cyclic thiourea functionalized dyes with binary π-linkers: influence of different π-conjugation segments on the performance of dye-sensitized solar cells. Dyes Pigments 2015;116:146–54.
[47] Yang J, He W, Denman K, Jiang Y-B, Qin Y. A molecular breakwater-like tetrapod for organic solar cells. J Mater Chem 2015;3(5):2108–19.
[48] Chen R, Yang X, Tian H, Wang X, Hagfeldt A, Sun L. Effect of tetrahydroquinoline dyes structure on the performance of organic dye-sensitized solar cells. Chem Mater 2007;19(16):4007–15.
[49] Li R, Liu J, Cai N, Zhang M, Wang P. Synchronously reduced surface states, charge recombination, and light absorption length for high-performance organic dye-sensitized solar cells. J Phys Chem B 2010;114(13):4461–4.
[50] Ellis H, Vlachopoulos N, Häggman L, Perruchot C, Jouini M, Boschloo G, et al. PEDOT counter electrodes for dye-sensitized solar cells prepared by aqueous micellar electrodeposition. Electrochim Acta 2013;107:45–51.
[51] Fabregat-Santiago F, Bisquert J, Palomares E, Otero L, Kuang D, Zakeeruddin SM, et al. Correlation between photovoltaic performance and impedance spectroscopy of dye-sensitized solar cells based on ionic liquids. J Phys Chem C 2007;111(17):6550–60.